Fernández-Benavides, D.; Cervera-Chiner, L.; Jiménez Jiménez, Y.; Arias De Fuentes, O.; Montoya, Á.; Muñoz-Saldaña, J. (15-0). A novel bismuth-based lead-free piezoelectric transducer immunosensor for carbaryl quantification. Sensors and Actuators B Chemical. 285:423-430. https://doi.org/10.1016/j.snb.2019.01.081

A novel Bismuth-based lead-free piezoelectric transducer immunosensor for carbaryl quantification

D.A. Fernández-Benavides[1], L. Cervera-Chiner[2], Y. Jiménez[2,3], O. Arias de Fuentes[4], A. Montoya[2] and J. Muñoz-Saldaña[1*]

[1] Centro de Investigación y de Estudios Avanzados del IPN, Lib. Norponiente No.2000, Fracc. Real de Juriquilla, 76230, Querétaro, Qro. México.

[2] Centro de Investigación e Innovación en Bioingeniería (Ci[2]B), Universitat Politècnica de València, Camino de Vera s/n, 46022 Valencia, España.

[3] Advanced Wave Sensors S.L., Calle Algepser 24, 46988 Paterna, Valencia, España.

[4] Instituto de Ciencia y Tecnología de Materiales, Universidad de la Habana, Ciudad de la Habana, Cuba.

[*] *Corresponding Author: jmunoz@cinvestav.mx*

Abstract

A novel BNT-BKT-BT piezoelectric ceramic immunosensor, tested for quantification of the pesticide carbaryl is here presented. The measuring format was based on a competitive immunoassay of immobilized conjugate using monoclonal antibodies (MAbs) as specific immunoreagent. The immunosensor is able to detect concentrations of the analyte from one and up to three orders of magnitude below the reported values of high- and low- frequency quartz crystal commercial resonators (HFF-QCM and QCM), respectively. Furthermore, the minimum content of quantified carbaryl is 0.11 μg L^{-1}, which is clearly lower than reported values of any commercial quartz-based biosensors. Such measurement characteristics are only possible due to the high electromechanical coupling factor (k_t) of the Bi-based piezoelectric ceramic, approaching the commercial QCM, HFF-QCM, ELISA´s technique and strongly enhancing the sensitivity in the immunoassay.

Keywords: Immunosensor, lead-free piezoelectric ceramic, BNT-BKT-BT, carbaryl.

1. Introduction

Further progress in medical diagnosis, drug discovery, biotechnology and environmental control require more and more selective and sensitive measurements. During the last 20 years, several methods have been developed, including immunological methods, polymerase chain reaction (PCR) and biosensors [1]. Currently, both enzyme-linked immunosorbent assays (ELISA) and immunosensors [2] are the most common immunoassays. The ELISA method uses a biochemical recognition reagent that could compromise the biochemical activity [3,4]. A label-free immunosensor combines the selectivity of the immunological interactions with the high sensitivity of the electronic signal transducer [5–7]. Both are typically used for the monitoring of low molecular weight compounds in analytical devices such as impedance spectroscopy, surface plasmon resonance (SPR), cantilever-based, piezoelectric-based, among others [8].

A piezoelectric immunosensor works as a transducer through the resonance frequency, that is principally determined by the thickness of the transducer, which itself defines the sensitivity of the assay [9–11]. The transducer element commonly works in the micro-gravimetric mode and has been used as piezoelectric sensor since Günther Sauerbrey discovered the relationship between the mass deposited/absorbed in the surface of the material and variations in frequency [12]. These sensors are suitable for the detection of a broad range of analytes including bacteria and eukaryotic cells [10,13], viruses [14,15], proteins [16], nucleic acids [17] and small molecules such as drugs, hormones and pesticides [18,19] by using recognition ligands such as antibodies, aptamers (DNA or RNA molecules) and peptides that bind specifically and with high affinity to the analyte. The antibodies are the most commonly used, but the advances in selection methods for aptamers (SELEX) and peptides (phage and yeast display) provides alternatives, principally when the target molecules are not immunogenic, and the antibodies are difficult to generate [8].

Particularly, the pesticides are potentially harmful to human's health and the environment [20]. The minimum allowed pesticide concentration in water intended for human consumption is around 0.10 $\mu g \cdot L^{-1}$. There are several reports to detect low concentrations of dangerous pesticides through different immunological techniques such as, membrane-based competitive enzyme immunoassays in flow through for carbaryl, with a limit of detection

(LOD) of 10 μg L^{-1} [21], membrane-based in flow through / lateral flow for carbaryl and endosulfan with LODs of 10 μg L^{-1} and 1 μg L^{-1} respectively [22], a rapid enzyme immunoassay using 8-well coated stripes for carbaryl and methoprene with LODs of 1.09 mg L^{-1} and 0.99 mg L^{-1} respectively, a BELISA assay based on molecularly imprinted polymers on paper for carbaryl detection with a sensitivity (IC_{50}) of 0.116 mg L^{-1} [23], among others. The allowed pesticide concentration is also challenging to measure or even detect with the commercially available quartz-based biosensors [24–26], which are also the most commonly used piezoelectric transducers [11,27–29]. Based on Marrazza´s review about piezoelectric biosensors for organophosphate and carbamate pesticides, different efforts are currently being undertaken in several research groups to improve the limit of detection of QCM-based biosensors [30]. The piezoelectric biosensors are promising candidates to detect pesticides, seeking to enhance LOD by varying their working frequencies [31–33]. For instance, March *et al.* in 2009 [34] reported the use of a quartz-based piezoelectric immunosensor for the detection of the pesticide carbaryl and the metabolite 3,5,6-trichloro-2-pyridinol (TCP), based on the immobilization of the hapten - conjugate and monoclonal antibodies. This type of immunoassay evidenced to be between 10 to 100 times more sensitive compared to other biosensing techniques based on the inhibition of the enzyme acetylcholinesterase [34]. Subsequently, the same authors proposed a new electronic characterization approach based on the fixed-frequency phase-shift measurement technique previously described in Montagut *et al.* 2011 [2], to obtain a high-frequency quartz crystal immunosensor (HFF-QCM) as an alternative to increase the analytical performance and versatility of these sensors [35]. The results of the new high-frequency sensor (100 MHz) were compared with those of low-frequency (9 MHz) and evidenced an improvement in sensitivity and LOD. As mentioned before, sensitivity depends of the area of the electrodes and resonance frequency, the latter is directly affected by the thickness of the transducer. Nevertheless, reducing the thickness of a quartz crystal biosensor has a natural limit, since the preparation of thinner and smaller quartz-based transducers becomes increasingly challenging [36,37]. Thus, piezoelectric ceramic resonators are emerging as an alternative, offering advantages in manufacturing and costs due their multifunctional characteristics. However, biosensing applications have been rarely explored by polycrystalline piezoelectric ceramic transducers, such as lead zirconate

titanate ceramics (PZT) due to its remarkable ferro/piezoelectric properties [38–41]. There are few reports claiming that PZT-based piezoelectric ceramics were successfully used as immunosensors, e.g. working as low-frequency resonators (< 200 kHz), exhibiting a narrow range for detection of the prostate-specific antigen (PSA) by frequency shifts [39] and quantification of fructose in aqueous solution [40]. A high-frequency (40 MHz) PZT-based biosensor has been reported to detect PSA and alpha-fetoprotein (AFP), with *LODs* around 0.25 ng L^{-1} [38]. Moreover, PZT-based ceramics were also used as mass sensors to measure the intraocular pressure in an *in vitro* pig eye [41].

However, the use of PZT is controversial because of its toxicity due to the high PbO vapor pressure during sintering steps of functional devices [42,43], as well as its instability when used or released in aqueous environments [44]. Apart from the well-known barium titanate $BaTiO_3$ (BT), other lead-free perovskites are considered as candidates to replace PZT systems [45–47], such as bismuth-sodium titanate $(Bi_{0.5}Na_{0.5})TiO_3$ (BNT), bismuth-potassium titanate $(Bi_{0.5}K_{0.5})TiO_3$ (BKT) and their respectively quasi-binary and quasi-ternary combinations with BT, which are well described elsewhere [48–50]. The reported piezoelectric properties from the ternary system BNT-BK-BT are already comparable with PZT [48,51]. Despite the lead-free piezoelectric bismuth-based ceramics already have shown adequate properties to replace lead-based materials, there are surprisingly no reports in the literature on their use in biosensing applications.

In this work, a lead-free bismuth-based piezoelectric ceramic with high electromechanical properties was previously fabricated following a method based on mixed oxides and carbonates and subsequently solid state reaction [52]. The sintered ceramic was thereafter conditioned to develop a novel immunosensor for a typical dangerous pesticide: The N-methylcarbamate insecticide carbaryl. A preliminary carbaryl calibration curve was obtained from competitive immunoassays after functionalization and immobilization of the gold deposited layer on the surface of the ceramic. In addition, the lead-free ceramic biosensor was compared with low (QCM) and high-frequency (HFF-QCM) commercial quartz crystals. Summarized details of the analytical parameters of interest such as *LOD*, I_{50} and working range are here presented and discussed.

2. Materials and methods

2.1 Ceramic preparation

Highly dense lead-free piezoelectric ceramics were prepared in a composition of $95(Bi_{0.5}Na_{0.5})TiO_3 + 2.5(Bi_{0.5}K_{0.5})TiO_3 + 2.5(BaTiO_3)$ by mixing commercial oxides and carbonates such as Bi_2O_3, TiO_2, $BaCO_3$ (Sigma Aldrich, St. Louis, MO, USA), Na_2CO_3 (Meyer, CDMX, Mexico), and K_2CO_3-$1.5H_2O$ (J.T. Baker, J. T. Baker Chemical, Phillipsburg, NJ, USA), all of them with purity over 99.5 %. Stoichiometric amounts of the mixed oxides were ball milled in a planetary system with methanol and Y_2O_3 - stabilized zirconia balls as grinding media based on 2:1 and 10:1 methanol (mL) to powder (g) and ball to powder ratio, respectively. Furthermore, mixed powders were dried at 100 ºC for 24 h and subsequently calcined at 920 ºC for 5 h. Thereafter, the calcined powder was manually milled in a mortar for 10 minutes. This calcination procedure was carried out by triplicate to assure a full solid-state reaction for the synthesis of the Perovskite.

An additional ball milling step using a SPEX 8000D mixer mill was undertaken and the product was sieved with a 44 μm mesh. Thereafter, disc-shaped green samples were uniaxial pressed with 3.4 MPa using a hardened steel die of 16.5 mm in diameter and then sintered at 1120 ºC for 5 h. Finally, the thickness of sintered ceramics was reduced to a 270 μm. Gold electrodes were deposited on sintered ceramics by a mini-sputtering system (LVC-76, Plasma Sciences).

2.2 Sample Characterization.

The crystalline structure of the sintered samples was characterized by X-ray diffraction by using a Rigaku Dmax 2100 diffractometer (Rigaku Corp, Tokyo, Japan), CuKα radiation (λ = 1.5406 Å) and a step size of 0.02◦.

The microstructure of sintered ceramics was recorded using a field emission scanning electron microscope, FESEM JEOL 7610F (Tokyo, Japan).

Ceramic transducers were obtained after poling at room temperature, applying an electric field of 50 kV cm^{-1} using a voltage direct current (VDC) source at 1.4 kV for 1 h, embedded in silicone oil to prevent dielectric breakdown. Piezoelectric coefficient (d_{33}),

capacitance (C_0) and dissipation factor ($tan\ \delta$) were measured in the transducers using a piezometer device (Piezotest PM300). The electric minimum impedance (Z_{min}) in the resonance (f_r) – antiresonance (f_a) frequencies and conductance (G) in thickness mode were obtained by using a Keysight E4990A impedance analyzer. The quality factor (Q_m) and electromechanical coupling thickness factor (k_t) constants were calculated according to following expressions:

$$Q_m = \frac{1}{4\pi C_0 Z_{min} \Delta f} \quad \text{Eq. (1)}$$

$$k_t = \sqrt{\frac{\pi f_r}{2 f_a} tan\left(\frac{\pi}{2}\frac{(f_a - f_r)}{f_a}\right)} \quad \text{Eq. (2)}$$

Ceramic transducers were placed in a test flow cell and subsequently analyzed in an acoustic platform from Advanced Wave Sensors S.L. (AWSensors). Conductance were measured in dry and at continuous water flow of 20 µL min^{-1}.

2.3. Ceramic biosensor prototype

Before transducer functionalization, a cleaning protocol to eliminate the traces of dielectric oil from the polarization process on the piezoelectric ceramics was carried out. First, the sensors were immersed for 5 min in a solution of 25 % NH_4OH in distilled water, at 75 ºC with continuous magnetic stirring. Thereafter, the ceramic was subjected to the following cleaning sequence: rinsing with bi-distilled water and ethanol, drying with nitrogen gas, exposure to UV radiation/ozone in a ProCleaner device (Bioforce Nanosciences) for 20 min, and a final rinsing step. After the cleaning protocol a transducer functionalization and immobilization protocols were undertaken, which are schematically shown in figure 1.

2.3.1 Transducer functionalization

The immunoreagents used in the immunosensor consisted of a protein-hapten conjugate (BSA-CNH) for covalent immobilization and a monoclonal antibody (MAb: LIB-CNH45) for the specific immunoassay (Figure 1a), both prepared at Ci2B (UPV) as previously described [20].

The ceramic sensors surface functionalization was performed through a mixed self-assembled monolayer (mSAM) composed by alkane thiols as intermediate layers (Figure 1a), following slight modification of the protocols reported elsewhere [34,35]. Briefly, thiolated compounds for the mSAM formation were 11-Mercapto-1-decanol (MUOH) and 16-Mercaptohexadecanoic acid (MHDA) (Sigma-Aldrich), at a 50:1 ratio and a total concentration of 10 mM in ethanol. BSA-CNH conjugate in 0.1 M sodium phosphate buffer, pH 7.5, was assayed at 0, 0.2, 0.5 and 1 mg mL^{-1} concentrations and it was incubated for 2.5 h to allow covalent immobilization (Figure 1b). Finally, sensors were air-dried and stored at 4 ºC.

2.3.2 Immunoassay protocol

Commercial carbaryl pesticide (Dr. Ehrenstorfer-GmbH) was used as a contaminant reference model analyte. The working conditions to quantify carbaryl with 9 MHz quartz crystal sensors were previously reported [34].

A 1 mM stock solution of carbaryl was prepared in dimethylformamide and stored at -20 ºC. After that, carbaryl standard solutions ranging from 4000 to $4x10^{-4}$ µg L^{-1} were prepared by serial dilutions in PBS (10 mM phosphate buffer solution, 0.9 % NaCl, pH 7.4). The working buffer consisting of PBST (PBS containing 0.005 % of surfactant Tween-20) was flowed through the sensor to reach a baseline. A suitable baseline was considered when the sensor signal (phase variation at fixed fundamental frequency $\Delta u\phi$) were lower than 1 mV min^{-1}.

Carbaryl standard solutions (375 µL) were mixed with an equal volume of LIB-CNH45 monoclonal antibody to carbaryl (10 µL mL^{-1}) and subsequently incubated for 1 h at 25 ºC to perform the competitive immunoassays (Figure 1c,f). Thereafter, 250 µL of the pre-incubated sample was injected and allowed to interact with the functionalized sensor surface for 20 min, with a continuous working buffer flow rate of 20 µL min^{-1} (Figure 1d,g). All standard concentrations were run at least in duplicate.

The regeneration of the biosensor surface was performed with 0.1 M HCl pumped at 250 µL min^{-1} for 4 min, followed by working buffer at 250 µL min^{-1} for 5 min to break the

antibody-hapten conjugate binding. Then the flow rate was re-established to 20 µL min^{-1} to recover the baseline.

Specific analytical parameters of the carbaryl standard calibration curve were calculated by plotting the phase shift vs analyte concentration, and fitting the experimental points to the following four-parameter logistic equation (*Eq. 3*), using Sigmaplot ® software:

$$y = D + \frac{A - D}{1 + \left(\frac{x}{C}\right)^{B}} \qquad \text{Eq. (3)}$$

where *x* and *y* are the analyte concentration and the assay signal (The normalized phase voltage variation 100x $\Delta u\phi/\Delta u\phi_0$ where $\Delta u\phi_0$ is the phase voltage variation at zero analyte concentration, or maximum signal), respectively. *A* is the maximum asymptote (maximum signal in the absence of analyte), *B* is the slope of the sigmoidal curve at the inflection point *C*, the latter represents the analyte concentration providing 50 % of inhibition (I_{50} value), and *D* is the minimum asymptote (minimum signal at saturating analyte concentrations)

2.3.3 Acoustic sensor platform (AWS A20-F20)

For the immunochemical assays, a platform from AWSensors including AWS-A20 and AWS-F20 research and fluidic modules was used. The piezoelectric immunosensors were placed into a flow cell (also from AWSensors) with the mechanical and electrical requirements for this application (Figure 2a). The flow cell was connected to the AWS-A20 module (Figure 2b).

AWS-A20 module has previously been used to characterize the sensor response during the experiments performed in flow conditions. This platform consists of an electronic characterization system based on the fixed-frequency phase-shift measurement technique described elsewhere [2,34,35], and provides two electrical voltages directly related with the sensor phase and amplitude ($u\phi$ and uA). The AWS-F20 platform has been used to generate a uniform flow through the sensor cell and consists on automated flow-through equipment controlled by syringe pumps (Hamilton, Bonaduz, GR, Switzerland) and thermostatized at 25 °C. Sample injection is performed at a 250 µL. The AWSuite software interface from

AWSensors was used to control both platforms during the experiments and for data acquisition.

Before covalent immobilization of the conjugate, ceramic sensors were electronically characterized in the A20 platform to determine the impedance and conductance values. The operation frequency was set up so that the sensor showed the maximum conductance.

3. Results and discussion

3.1 BNT-BKT-BT ceramics

A typical diffraction pattern of the 95BNT-2.5BKT-2.5BT ceramics is shown in figure 3a, where the perovskite-type structure and a rhombohedral phase without presence of secondary phases when compared with a theoretical PDF (ISCD 98-006-3231) was confirmed. This rresult is consistent with literature data since compositions of (97.5 – *x*)BNT-*x*BKT-2.5BT with *x* between 0 - 9 mol% BKT crystallize with *Rc3* rhombohedral symmetry [52].

On the other hand, figure 3b shows a typical SEM micrograph of the 95BNT-2.5BKT-2.5BT sample recorded with a secondary electrons detector. These ceramics show a equiaxial shaped grains with 2.35 μm average size. This microstructure is also in agreement with previous reports [52,53]. It is worth to mention that the sintered ceramics evidence a densification over 95 % of the theoretical density as measured by the Archimedes method that matches with the low porosity observed in the micrograph of figure 2b.

It is well-known that the microstructural characteristics of BNT-BKT-BT ceramics are directly related with their piezoelectric behavior [52,54]. As mentioned before, the piezoelectric properties of the 95BNT-2.5BKT-2.5BT ceramics were obtained from the impedance module in a frequency range presented in figure 4a. The measured values for the characteristic pair of resonance f_r, f_a and Z_{min} of the poled ceramic were 6.7 MHz, 7.1 MHz and 20.4 Ω, respectively. In this case, Q_m and k_t were calculated by following the resonance frequencies method and using equations 1 and 2. Table 1 summarizes the piezoelectric constants k_t, Q_m and d_{33} exhibiting a value of 0.37, 15.88 and 75 pC/N, respectively.

Finally, both the electrical phase (Figure 4b) and the conductance (Figure 4c) were used to establish the work-resonance frequency (W_rf). The poled ceramic evidences an inductive behavior (Figure 4b) at a frequency of 6.92 MHz. Moreover, the maximum conductance (0.05 S) is reached at 6.7 MHz (Figure 4c), which also represents the piezoelectric moment of the ceramic with lower losses. Thus, the used $Wrf = f_r$ = 6.7 MHz.

3.2 Biosensor behavior

3.2.1 Immunoassay format

An indirect competitive (inhibition) immunoassay was employed to quantify carbaryl in the conjugate-coated format. For the inhibition assays, a fixed concentration of the specific monoclonal antibody was first mixed and incubated with the same volume of the standard analyte solution. Thereafter, the incubated mixture was pumped over the immunosensor surface to complete the immunoassay. Both, phase and amplitude ($u\phi$ and uA) variations were continuously monitored as analytical assay signals. Figure 1e shows a schematic representation of the phase voltage signal expected to be obtained in a functionalized and immobilized piezoelectric sensor that was subsequently put in contact with the antibody-analyte mixture. Figure 1a and 1b represent the schematic of the functionalized transducer with a given concentration of immobilized hapten conjugate on its surface. In figure 1c, a sample with only free MAb was pumped on the surface of the sensor. As a consequence, all available MAb molecules will bind to the immobilized conjugate on the sensor surface (Figure 1d), leading to the characteristic decrease of the phase voltage in figure 1e (maximum assay signal in the absence of analyte). A phase voltage decrease of approximately 100 mV is usually considered as a good signal for a successful quantification. Such a signal correlates to the minimum detectable concentration of antibody and immobilized conjugate on the biosensor surface and contributes to the sensitivity of the device, reflected in the analytical parameters of interest such as the limit of detection (*LOD*), limit of quantification (*LOQ*) and 50 % inhibition value (I_{50}).

The opposite situation, in figure 1f a sample with very high analyte concentration (MAb <<< Analyte) is pumped on the surface of the biosensor after incubation. The limited available MAb molecules will preferentially bind to the analyte in solution rather than to the immobilized conjugate on the sensor surface (Figure 1g), leading to the inhibition signal

presented in figure 1h. It is well known that the viscosity of the samples also modifies the base-line of the phase voltage. Nevertheless, phase voltage shifts lower than 25 mV were still considered as useful inhibition signals. In the high-frequency piezoelectric transducers, the viscosity effect does not influence the inhibition signal so that, can be considered negligible [34,35].

In a competitive assay, once the maximum and inhibition signal is settled up, the phase voltage or resonance frequency shifting of samples with different concentrations of analyte in the operative working range is measured. Subsequently, a calibration curve to determine the analytical parameters of interest for the quantification of the analyte can be obtained by plotting the phase voltage shift versus the analyte concentration. Typical calibration curves of competitive immunoassays and immunosensors show a decreasing sigmoidal shape because the assay signal decreases as the analyte concentration does.

3.2.2 Dose – response analysis

For the determination of the optimal concentrations of immunoreagents to perform immunochemical assays and further calibration curve for carbaryl, several concentrations from 0.2 to 1 mg mL^{-1} of BSA-CNH conjugate were first immobilized on the ceramic surface and tested in combination with different concentrations of monoclonal antibody to carbaryl (LIB-CNH45 MAb between 0 and 20 µg mL^{-1}). Ceramic sensors immobilized with only BSA and 0 mg mL^{-1} of BSA-CNH conjugate worked as a negative control to assure that signal shifts were only due to the specific binding of the antibody to the immobilized conjugate on the surface of the sensor.

A procedure to determine the optimal combination of the immobilized hapten conjugate and monoclonal antibody concentrations was developed to obtain signals of at least 100 mV with the lowest immunoreagent consumption. The signals provided by each immunoreagent combination are summarized in table 2. As expected, higher signals were observed as MAb and conjugate concentrations increased. The fluctuations in some experiments are probably due to the polycrystalline nature of the piezoelectric ceramics such as microstructure, porosity and other defects associated to the used processing route that directly affects the electromechanical behavior, e.g. the low values of Q_m that results in high responses variance. According to these results, the selected concentrations to perform

311 the calibration curve for carbaryl were: 0.2 mg mL^{-1} of the immobilized BSA-CNH
312 conjugate and 20 μg mL^{-1} of LIB-CNH45 monoclonal antibody.

313 It is worth to remark that for BNT-BKT-BT ceramic sensors, the required concentration of
314 the used immobilized conjugate to reach convenient measurement signals was one order of
315 magnitude below that reported for commercial low-frequency (9 MHz) quartz crystal
316 resonators (QCM) [34]. This effect is probably due to the high electromechanical coupling
317 factor in the thickness of the BNT-BKT-BT ceramics compared to the quartz crystal
318 sensors, tending to decrease the consumption of costly immunoreagents. A comparison
319 between the properties of interest of the BNT-BKT-BT piezoelectric ceramic with low and
320 high-frequency commercial quartz crystal microbalances used for biosensing applications is
321 shown in Table 1.

322 The following observations can be done considering that the piezoelectric factors k_t and Q_m,
323 are inversely proportional to each other and that their values determine how the
324 immunoassay will be measured, either by frequency changes or phase voltage shift.

325 The electromechanical coupling factor k_t (thickness mode) of the BNT-BKT-BT
326 piezoelectric ceramic is higher than those from either QCM or HFF-QCM. As a
327 consequence, significant phase voltage variations are expected as a function of small mass
328 changes on the surface of the ceramic transducer. The opposite situation is observed for the
329 mechanical quality factor Q_m, where the BNT-BKT-BT piezoelectric ceramic exhibits a
330 very low Q_m value compared to QCM and HFF-QCM. In this case, mass changes in the
331 surface imply small variations in frequency that can only be observed by a piezoelectric
332 transducer with high Q_m performance.

333 ***3.2.3 Standard calibration curve***

334 The successful quantification of the immunological reactions that produces mass changes in
335 the surface of the biosensor, requires the construction of a standard calibration curve for the
336 analyzed compound. In this particular case, the obtained calibration curve for carbaryl with
337 a BNT-BKT-BT lead-free piezoelectric ceramic immunosensor is given in figure 5. Each
338 point of the curve represents the average of two replicates and corresponds to the assay
339 signal (sensor response as phase voltage shift) produced by carbaryl standard solutions (0,

0.2, 2, 20, 200, 2000 µg L^{-1}) subjected to the competitive assay with a fixed concentration of MAb. Assay signals are normalized with respect to the reference one, which corresponds to zero analyte concentration (only MAb).

As expected, the competitive nature of the immunoassay is reflected in the sigmoidal behavior of the standard curve. From figure 5 it becomes clear that the signal decreases as an inverse function of the analyte concentration, which reduces the quantity of free available antibody molecules in the assay leading to a proportional inhibition. In the point with the highest assayed analyte concentration (2000 µg L^{-1}) and as mentioned before, data with higher standard deviation (that correspond to the inhibition signal) may be influenced by a viscosity effect [34].

The analytical parameters of the carbaryl calibration curve were calculated by fitting the experimental data to the above described four-parameter equation (*Eq. 3*). The I_{50} value is the most characteristic parameter of immunoassay standard curves since it estimates the assay sensitivity and hence defines the analytical quality of the calibration curve. Lower I_{50} values suggest an enhancement of the biosensor sensitivity and are directly related to the lower concentration of analyte needed to produce 50 % of the signal inhibition. In this case, the I_{50} value was 1.15 µg L^{-1} of carbaryl. On the other hand, the precision of this immunoassay resembles the one reported for the ELISA method [2].

3.2.4 Comparison with commercial biosensors

Table 3 summarizes the analytical parameters for the carbaryl standard curve of the BNT-BKT-BT-based biosensor, in comparison to commercial QCM and HFF-QCM biosensors.

From table 3 it can be observed that the limit of detection (*LOD* = 0.03 μg L^{-1}) of the BNT-BKT-BT biosensor is three orders of magnitude below QCM 1 (*LOD* = 13.30 μg L^{-1}) and two orders of magnitude below QCM 2 (*LOD* = 4.00 μg L^{-1}) [34]. The *LOD* was even one order of magnitude lower than HFF-QCM (0.23 and 0.14 μg L^{-1}) [35]. On the other hand, the BNT-BKT-BT immunosensor exhibits an I_{50} = 1.15 μg L^{-1}, being one order of magnitude below QCM 1 and QCM 2 (30.34 and 16.70 μg L^{-1}, respectively), and even lower than HFF-QCM 1 (1.95 μg L^{-1}). Moreover, the working range (0.11 - 11.68 μg L^{-1}) for carbaryl quantification exhibited by the BNT-BKT-BT biosensor is wider than in QCM

1 (18.30 - 50.30 μg L^{-1}), QCM 2 (7.00 - 35.00 μg L^{-1}), HFF-QCM 1 (0.5 - 7.20 μg L^{-1}) and HFF-QCM 2 (0.26 - 1.72 μg L^{-1}), since it covers a range of two orders of magnitude between the lower and upper limits [34,35]. Finally, considering the calculated working ranges, the BNT-BKT-BT immunosensor evidenced a capability for carbaryl quantification in at least two and one order of magnitude lower than QCM 1 and QCM 2, respectively [34] and at lower concentrations than HFF-QCM quartz crystals [35].

Again, the successful biosensing response of the BNT-BKT-BT transducer is due to its high electro-mechanical transduction (k_t) that defines the sensitivity of the device. Our current results show that the working frequencies and dimensions of the BNT-BKT-BT biosensor overlap with those of QCM but with clearly a higher performance tending to be similar to the HFF-QCM responses. However, HFF-QCM devices are much more difficult to handle due to the extremely low dimensions to reach high working frequencies [34,35]. Nevertheless, and as mentioned before, a natural limit can be anticipated related to the challenge in manufacturing thinner quartz transducers.

The present work presents a specific composition of a Bi-based piezoelectric ceramic for a targeted biosensing application. The broad range of BNT-BKT-BT compositions that can be used for these applications can lead to vary the electromechanical behavior, decrease the electrical losses, avoid the internal micro-defects and enhance the overall quality of the biosensing properties. Systematic studies such as design of experiments involving mixtures design or simultaneous optimization techniques need to be done to establish the effect of BNT, BKT and BT compositions on the structural, microstructural, dielectric, ferroelectric and piezoelectric properties of sintered ceramics seeking to enhance their biosensing response.

Conclusions

A specific composition of a BNT-BKT-BT (95BNT-2.5 BKT-2.5 BT) piezoelectric ceramic immunosensor successfully detected and quantified carbaryl pesticide. The tested device was able to provide reliable signals with concentrations of the immobilized conjugate one order of magnitude lower than the reported values using biosensors based on commercial low-frequency quartz crystal resonators (QCM). This fact was considered in

399 the sensitivity assay for the pesticide carbaryl model, whose calculated sensitivity
400 parameters (I_{50} value and *LOD*) were 1.15 μg L^{-1} and 0.029 μg L^{-1}, respectively.

401 However, there is a lot of room to extend the sensing capabilities of the BNT-BKT-BT
402 transducers beyond those of HFF-QCM by optimizing their electromechanical factors. e.g.
403 by including advanced manufacture techniques, such as additive manufacturing, more
404 complex perovskites, or optimizing the structural, microstructural and chemical properties
405 of single-phase perovskites.

406 It is worth to point out that, to the author´s knowledge, no bismuth-based lead-free
407 piezoelectric ceramic transducer has been previously reported and successfully tested as
408 immunosensor potentially capable of quantifying a broad range of analytes, including the
409 present case of a harmful pesticides.

410

411 **Acknowledgments:** This project received support from CONACyT (Grants Nr. CB-
412 220734, FC 2015-2-896, LN 292686 and 293429). This work has been carried out at
413 CENAPROT and LIDTRA national laboratories as well as at Center for Research and
414 Innovation in Bioengineering (Ci2B) of Universitat Politècnica de València.

415

416 **Conflicts of Interest:** Authors confirm that the content of this article has no conflict of
417 interest.

418

REFERENCES

[1] A.K. Deisingh, M. Thompson, Biosensors for the detection of bacteria, Can. J. Microbiol. 50 (2004) 69–77. doi:10.1139/w03-095.

[2] Y. Montagut, J. V. García, Y. Jiménez, C. March, Á. Montoya, A. Arnau, Validation of a phase-mass characterization concept and interface for acoustic biosensors, Sensors. 11 (2011) 4702–4720. doi:10.3390/s110504702.

[3] S.S. Iqbal, M.W. Mayo, J.G. Bruno, B. V Bronk, C.A. Batt, J.P. Chambers, A review of molecular recognition technologies for detection of biological threat agents, Biosens. Bioelectron. 15 (2000) 549–578. doi:10.1016/S0956-5663(00)00108-1.

[4] B.E. Hawkins, M. Cooper, I. Campbell, Acoustic Detection Technology in the Analysis of Biomolecular Interactions, (2006) 30–33.

[5] A. Arnau, Piezoelectric Transducers and Applications, Second Edition, Springer-Verlag New York, Valencia, 2008. doi:10.1007/978-3-540-77508-9.

[6] M.P. Byfield, R.A. Abuknesha, Biochemical aspects of biosensors, Biosens. Bioelectron. 9 (1994) 27. doi:10.1016/0956-5663(94)80038-3.

[7] J.L. Marty, B. Leca, T. Noguer, Biosensors for the detection of pesticides, Analusis. 26 (1998) 144–148. doi:10.1051/analusis:199826060144.

[8] J.M. Walker, Biosensors and Biodetection Methods and Protocols Volume 504: Electrochemical and Mechanical Detectors, Lateral Flow and Ligands for Biosensors, Humana Press, New York, 2009. doi:10.1007/978-1-60327-569-9.

[9] A. Janshoff, H.J. Galla, C. Steinem, Piezoelectric mass-sensing devices as biosensors - An alternative to optical biosensors?, Angew. Chemie - Int. Ed. 39 (2000) 4004–4032. doi:10.1002/1521-3773(20001117)39:223.0.CO;2-2.

[10] Y.S. Fung, Y.Y. Wong, Self-assembled monolayers as the coating in a quartz piezoelectric crystal immunosensor to detect Salmonella in aqueous solution, Anal. Chem. 73 (2001) 5302–5309. doi:10.1021/ac010655y.

[11] X. Su, F. Tim Chew, S.F.Y. Li, Piezoelectric quartz crystal based label-free analysis for allergy disease, Biosens. Bioelectron. 15 (2000) 629–639. doi:10.1016/S0956-5663(00)00112-3.

[12] G. Sauerbrey, Verwendung von Schwingquarzen zur Wägung dünner Schichten und zur Mikrowägung, Zeitschrift Für Phys. 155 (1959) 206–222. doi:10.1007/BF01337937.

[13] Z. Fohlerová, P. Skládal, J. Turánek, Adhesion of eukaryotic cell lines on the gold surface modified with extracellular matrix proteins monitored by the piezoelectric sensor, Biosens. Bioelectron. 22 (2007) 1896–1901. doi:10.1016/j.bios.2006.08.015.

[14] J.S. Yu, H.X. Liao, A.E. Gerdon, B. Huffman, R.M. Scearce, M. McAdams, S.M. Alam, P.M. Popernack, N.J. Sullivan, D. Wright, D.E. Cliffel, G.J. Nabel, B.F. Haynes, Detection of Ebola virus envelope using monoclonal and polyclonal antibodies in ELISA, surface plasmon resonance and a quartz crystal microbalance immunosensor, J. Virol. Methods. 137 (2006) 219–228. doi:10.1016/j.jviromet.2006.06.014.

[15] X. Su, S.F.Y. Li, W. Liu, J. Kwang, Piezoelectric quartz crystal based screening test for porcine reproductive and respiratory syndrome virus infection in pigs, Analyst. 125 (2000) 725–730. doi:10.1039/a909415f.

[16] G. Shen, H. Wang, S. Tan, J. Li, G. Shen, R. Yu, Detection of antisperm antibody in human serum using a piezoelectric immunosensor based on mixed self-assembled monolayers, Anal. Chim. Acta. 540 (2005) 279–284. doi:10.1016/j.aca.2005.03.035.

[17] K. Feng, J. Li, J.H. Jiang, G.L. Shen, R.Q. Yu, QCM detection of DNA targets with single-base mutation based on DNA ligase reaction and biocatalyzed deposition amplification, Biosens. Bioelectron. 22 (2007) 1651–1657. doi:10.1016/j.bios.2006.07.023.

[18] N. Kim, I.S. Park, D.K. Kim, High-sensitivity detection for model organophosphorus and carbamate pesticide with quartz crystal microbalance-precipitation sensor, Biosens. Bioelectron. 22 (2007) 1593–1599. doi:10.1016/j.bios.2006.07.009.

[19] H. Sun, Y. Fung, Piezoelectric quartz crystal sensor for rapid analysis of pirimicarb residues using molecularly imprinted polymers as recognition elements, Anal. Chim. Acta. 576 (2006) 67–76. doi:10.1016/j.aca.2006.04.058.

[20] A. Abad, J. Primo, A. Montoya, Development of an Enzyme-Linked Immunosorbent Assay to Carbaryl. 1. Antibody Production from Several Haptens and Characterization in Different Immunoassay Formats, J. Agric. Food Chem. 45 (1997) 1486–1494. doi:10.1021/jf9506904.

[21] S. Wang, C. Zhang, Y. Zhang, Development of a flow-through enzyme-linked immunosorbent assay and a dipstick assay for the rapid detection of the insecticide carbaryl, Anal. Chim. Acta. 535 (2005) 219–225. doi:10.1016/j.aca.2004.12.009.

[22] C. Zhang, Y. Zhang, S. Wang, Development of multianalyte flow-through and lateral-flow assays using gold particles and horseradish peroxidase as tracers for the rapid determination of carbaryl and endosulfan in agricultural products, J. Agric. Food Chem. 54 (2006) 2502–2507. doi:10.1021/jf0531407.

[23] C. Zhang, H. Cui, Y. Han, F. Yu, X. Shi, Development of a biomimetic enzyme-linked immunosorbent assay based on molecularly imprinted polymers on paper for the detection of carbaryl, Food Chem. 240 (2018) 893–897. doi:10.1016/j.foodchem.2017.07.109.

[24] J.M. Abad, F. Pariente, L. Hernandez, H.D. Abruña, E. Lorenzo, Determination of organophosphorus and carbamate pesticides using a biosensor, Anal. Chem. 70 (1998) 2848–2855. doi:10.1021/ac971374m.

[25] N.G. Karousos, S. Aouabdi, A.S. Way, S.M. Reddy, Quartz crystal microbalance determination of organophosphorus and carbamate pesticides, Anal. Chim. Acta. 469 (2002) 189–196. doi:10.1016/S0003-2670(02)00668-2.

[26] J. Wang, W. Liu, D. Chen, Y. Xu, L. Zhang, A micro-machined thin film electro-acoustic biosensor for detection of pesticide residuals, J. Zhejiang Univ. Sci. C. 15 (2014) 383–389. doi:10.1631/jzus.C1300289.

[27] Y. Zhang, F. Lin, Y. Zhang, H. Li, Y. Zeng, H. Tang, S. Yao, Quartz crystal

microbalance detection of DNA single-base mutation based on monobase-coded cadmium tellurium nanoprobe, Anal. Sci. 27 (2011). doi:10.2116/analsci.27.1229.

[28] C.J. Percival, S. Stanley, M. Galle, A. Braithwaite, M.I. Newton, G. McHale, W. Hayes, Molecular-imprinted, polymer-coated quartz crystal microbalances for the detection of terpenes, Anal. Chem. 73 (2001) 4225–4228. doi:10.1021/ac0155198.

[29] C. Yao, Y. Qi, Y. Zhao, Y. Xiang, Q. Chen, W. Fu, Aptamer-based piezoelectric quartz crystal microbalance biosensor array for the quantification of IgE, Biosens. Bioelectron. 24 (2009) 2499–2503. doi:10.1016/j.bios.2008.12.036.

[30] G. Marrazza, Piezoelectric biosensors for organophosphate and carbamate pesticides: A review, Biosensors. 4 (2014) 301–317. doi:10.3390/bios4030301.

[31] B.P. Stehrer, R. Schwödiauer, S. Bauer, I.M. Graz, P.D. Pollheimei, H.J. Gruber, High frequency QCM based sensor system for sensitive detection of dissolved analytes, Procedia Eng. 5 (2010) 835–837. doi:10.1016/j.proeng.2010.09.238.

[32] E. Uttenthaler, M. Schräml, J. Mandel, S. Drost, Ultrasensitive quartz crystal microbalance sensors for detection of M13-Phages in liquids, Biosens. Bioelectron. 16 (2001) 735–743. doi:10.1016/S0956-5663(01)00220-2.

[33] H. Yoshimine, T. Kojima, H. Furusawa, Y. Okahata, Small mass-change detectable quartz crystal microbalance and its application to enzymatic one-base elongation on DNA, Anal. Chem. 83 (2011) 8741–8747. doi:10.1021/ac202224d.

[34] C. March, J.J. Manclús, Y. Jiménez, A. Arnau, A. Montoya, A piezoelectric immunosensor for the determination of pesticide residues and metabolites in fruit juices, Talanta. 78 (2009) 827–833. doi:10.1016/j.talanta.2008.12.058.

[35] C. March, J. V. García, Á. Sánchez, A. Arnau, Y. Jiménez, P. García, J.J. Manclús, Á. Montoya, High-frequency phase shift measurement greatly enhances the sensitivity of QCM immunosensors, Biosens. Bioelectron. 65 (2015) 1–8. doi:10.1016/j.bios.2014.10.001.

[36] C.R. Bowen, H.A. Kim, P.M. Weaver, S. Dunn, Piezoelectric and ferroelectric materials and structures for energy harvesting applications, Energy Environ. Sci. 7 (2014) 25–44. doi:10.1039/c3ee42454e.

[37] J.F. Scott, Applications of modern ferroelectrics, Science (80-.). 315 (2007) 954–959. doi:10.1126/science.1129564.

[38] L. Su, L. Zou, C.C. Fong, W.L. Wong, F. Wei, K.Y. Wong, R.S.S. Wu, M. Yang, Detection of cancer biomarkers by piezoelectric biosensor using PZT ceramic resonator as the transducer, Biosens. Bioelectron. 46 (2013) 155–161. doi:10.1016/j.bios.2013.01.074.

[39] J.H. Lee, K.S. Hwang, J. Park, K.H. Yoon, D.S. Yoon, T.S. Kim, Immunoassay of prostate-specific antigen (PSA) using resonant frequency shift of piezoelectric nanomechanical microcantilever, Biosens. Bioelectron. 20 (2005) 2157–2162. doi:10.1016/j.bios.2004.09.024.

[40] M.I.S. Veríssimo, P.Q. Mantas, A.M.R. Senos, J.A.B.P. Oliveria, M.T.S.R. Gomes, Suitability of PZT ceramics for mass sensors versus widespread used quartz crystals,

Sensors Actuators, B Chem. 95 (2003) 25–31. doi:10.1016/S0925-4005(03)00397-6.

[41] A. Eklund, T. Bäcklund, O.A. Lindahl, A resonator sensor for measurement of intraocular pressure - Evaluation in an in vitro pig-eye model, Physiol. Meas. 21 (2000) 355–367. doi:10.1088/0967-3334/21/3/302.

[42] M. Esquivel-Gaon, S. Anguissola, D. Garry, A.D.C. Gallegos-Melgar, J.M. Saldaña, K.A. Dawson, A. De Vizcaya-Ruiz, L.M. Del Razo, Bismuth-based nanoparticles as the environmentally friendly replacement for lead-based piezoelectrics, RSC Adv. 5 (2015) 27295–27304. doi:10.1039/c5ra02151k.

[43] K.H. Härdtl, H. Rau, PbO vapour pressure in the Pb(Ti1−x)O3 system, Solid State Commun. 7 (1969) 41–45. doi:10.1016/0038-1098(69)90688-7.

[44] W.W. Wolny, European approach to development of new environmentally sustainable electroceramics, Ceram. Int. 30 (2004) 1079–1083. doi:10.1016/j.ceramint.2003.12.025.

[45] E. Aksel, J.L. Jones, Advances in lead-free piezoelectric materials for sensors and actuators, Sensors. 10 (2010) 1935–1954. doi:10.3390/s100301935.

[46] I. Coondoo, N. Panwar, A. Kholkin, Lead-free piezoelectrics: Current status and perspectives, J. Adv. Dielectr. 03 (2013) 1330002. doi:10.1142/S2010135X13300028.

[47] P.K. Panda, Review: Environmental friendly lead-free piezoelectric materials, J. Mater. Sci. 44 (2009) 5049–5062. doi:10.1007/s10853-009-3643-0.

[48] J. Rödel, W. Jo, K.T.P. Seifert, E.M. Anton, T. Granzow, D. Damjanovic, Perspective on the development of lead-free piezoceramics, J. Am. Ceram. Soc. 92 (2009) 1153–1177. doi:10.1111/j.1551-2916.2009.03061.x.

[49] S. Priya, S. Nahm, Lead-free piezoelectrics, Springer New York, New York, NY, 2013. doi:10.1007/978-1-4419-9598-8.

[50] T. Takenaka, H. Nagata, Y. Hiruma, Current developments and prospective of lead-free piezoelectric ceramics, Jpn. J. Appl. Phys. 47 (2008) 3787–3801. doi:10.1143/JJAP.47.3787.

[51] T.R. Shrout, S.J. Zhang, Lead-free piezoelectric ceramics: Alternatives for PZT?, J. Electroceramics. 19 (2007) 111–124. doi:10.1007/s10832-007-9047-0.

[52] D.A. Fernandez-Benavides, A.I. Gutierrez-Perez, A.M. Benitez-Castro, M.T. Ayala-Ayala, B. Moreno-Murguia, J. Muñoz-Saldaña, Comparative study of ferroelectric and piezoelectric properties of BNT-BKT-BT ceramics near the phase transition zone, Materials (Basel). 11 (2018) 361. doi:10.3390/ma11030361.

[53] M. Otoničar, S.D. Škapin, M. Spreitzer, D. Suvorov, Compositional range and electrical properties of the morphotropic phase boundary in the Na0.5Bi0.5TiO3-K0.5Bi0.5TiO3system, J. Eur. Ceram. Soc. 30 (2010) 971–979. doi:10.1016/j.jeurceramsoc.2009.10.006.

[54] Q. Yin, B. Zhu, H. Zeng, Microstructure, Property and Processing of Functionnal Ceramics, Springer-Verlag GmbH Berlin Heidelberg, Shangai, 2010. doi:10.1007/978-3-642-01694-3.

Table Caption

Table 1. Comparison of piezoelectric parameters between QCM, HFF-QCM and the used lead-free bismuth-based piezoelectric ceramic.

Table 2. Obtained signals with a BNT-BKT-BT ceramic sensor in the checkerboard titration of several concentrations of the immobilized BSA-CNH conjugate and LIB-CNH45 monoclonal antibody to carbaryl

Table 3. Analytical performance of BNT-BKT-BT lead-free piezoelectric ceramic compared with commercial carbaryl immunosensors (QCM and HFF-QCM).

Figure Caption

Fig. 1 Scheme of the competitive immunoassay principles and signal transduction strategy.

Fig. 2 Measurement platform (AWS A20 – F20) set up listed as a) Flow cell, b) A20 acoustic platform and c) F20 fluidic module.

Fig. 3 a) X-ray diffraction pattern and b) Scanning electron micrograph of the 95BNT-2.5BKT-2.5BT sintered sample with rhombohedral symmetry.

Fig. 4 a) Impedance module, b) electrical phase and, c) conductance of the 95BNT-2.5BKT-2.5BT poled sample, at the resonance frequency.

Fig. 5 Standard calibration curve for the pesticide carbaryl performed with the BNT-BKT-BT ceramic sensor under optimized conditions. Each point represents the average ± standard deviation of two replicates.

Table(s)

Table 1.

	Low frequency			High frequency	
Characteristics	**BNT-BKT-BT**	**QCM 1 [34]**	**QCM 2 [34]**	**HFF-QCM1 [35]**	**HFF-QCM2 [35]**
Manufacturer	This work		AWSensors		
Diameter (mm)	14	14	14	5	5
Thickness (μm)	277 - 320	167 - 270	167 - 270	13-20	13-20
Capacitance (F)	$5.85E^{-10}$	-	-	-	-
Tan δ	0.037	-	-	-	-
d_{33} *(pC/N)*	75	-	-	-	-
Frequency (MHz)	6.7	9	10	50	100
k_t	0.37	0.021	0.018	0.008	0.006
Q_m	15.88	35000	30000	50000	70000

Fernández-Benavides et al., 2018

Table 2.

Signal ΔuΦ (mV)					
BSA-CNH Conjugate	**LIB-CNH45 Monoclonal Antibody to carbaryl (μg mL^{-1})**				
(mg mL^{-1})	0	2.5	5	10	20
0	10	28	-	40	30
0.2	20	18	90	***159***	***160***
0.5	60	50	48	***130***	***130***
1	30	9	***187***	***244***	***430***

Fernández-Benavides et al., 2018

Table 3.

Analytical parameters (*μg L^{-1}*)	**BNT-BKT-BT**	**QCM 1 [34]**	**QCM 2 [34]**	**HFF-QCM 1 [35]**	**HFF-QCM 2 [35]**
LOD	0.03	13.30	4.00	0.23	0.14
I_{50}	1.15	30.34	16.70	1.95	0.66
WR	0.11 - 11.68	18.30 - 50.30	7.00 - 35.00	0.50 - 7.20	0.26 - 1.72

Fernández-Benavides et al., 2018

Figure(s)

Figure 1.

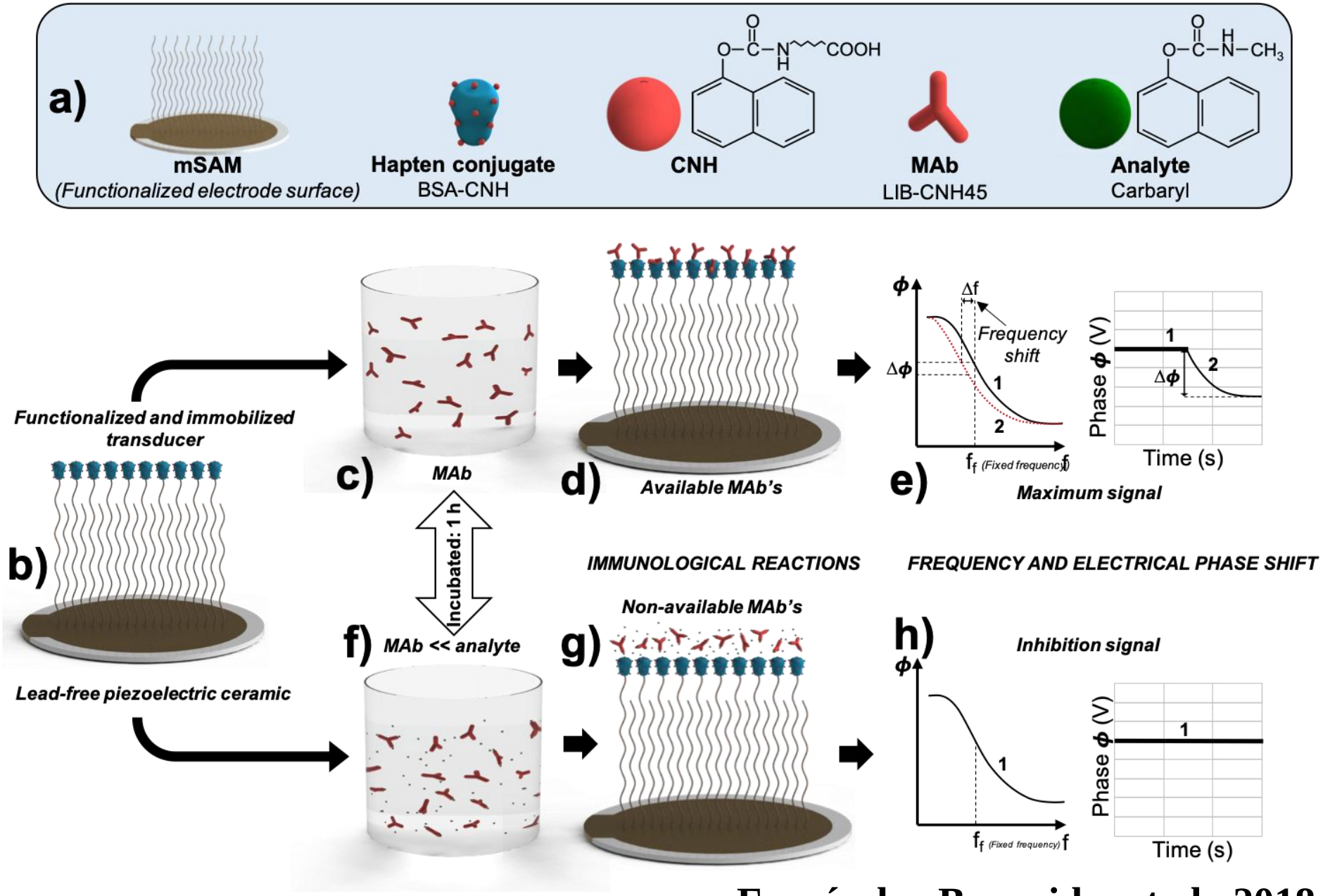

Fernández-Benavides et al., 2018

Figure 2.

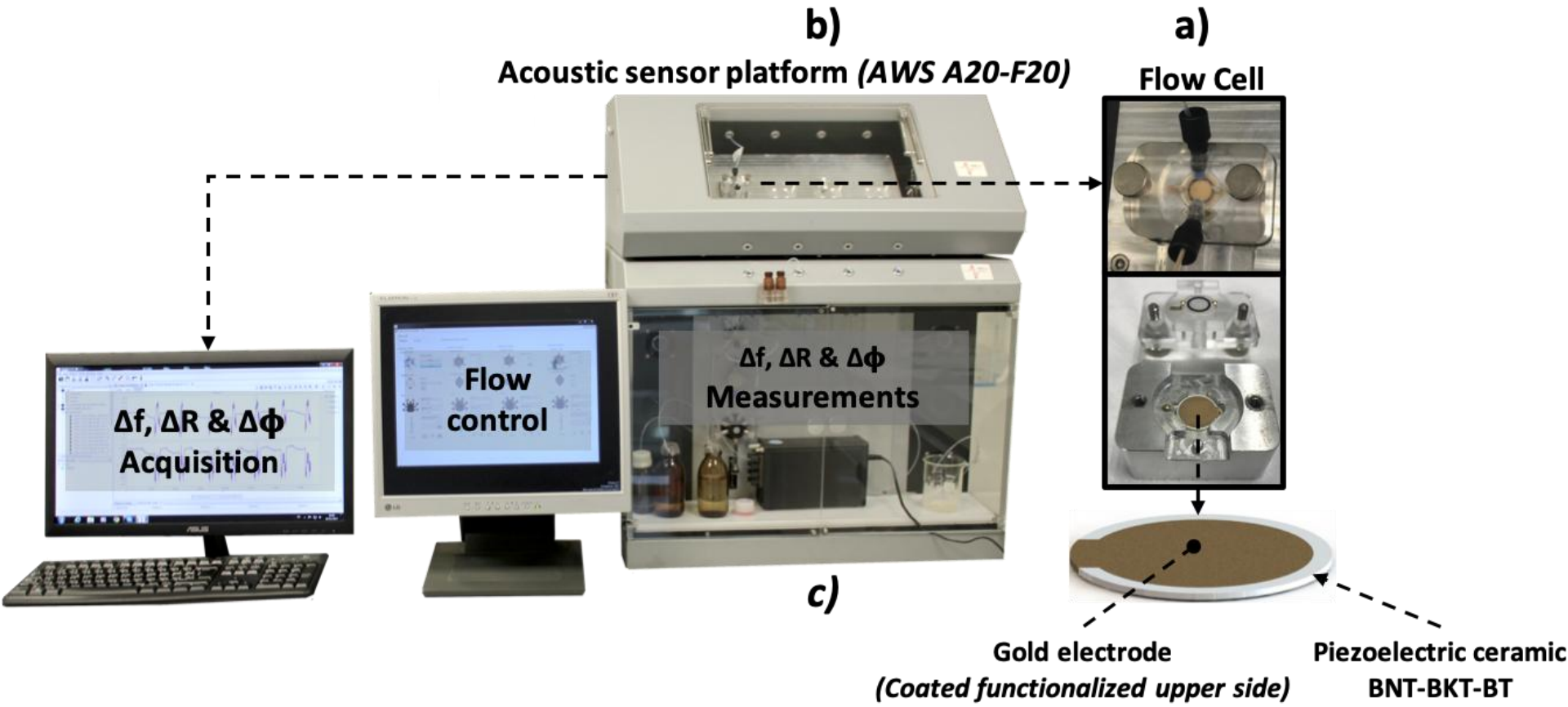

Fernández-Benavides et al., 2018

Figure 3.

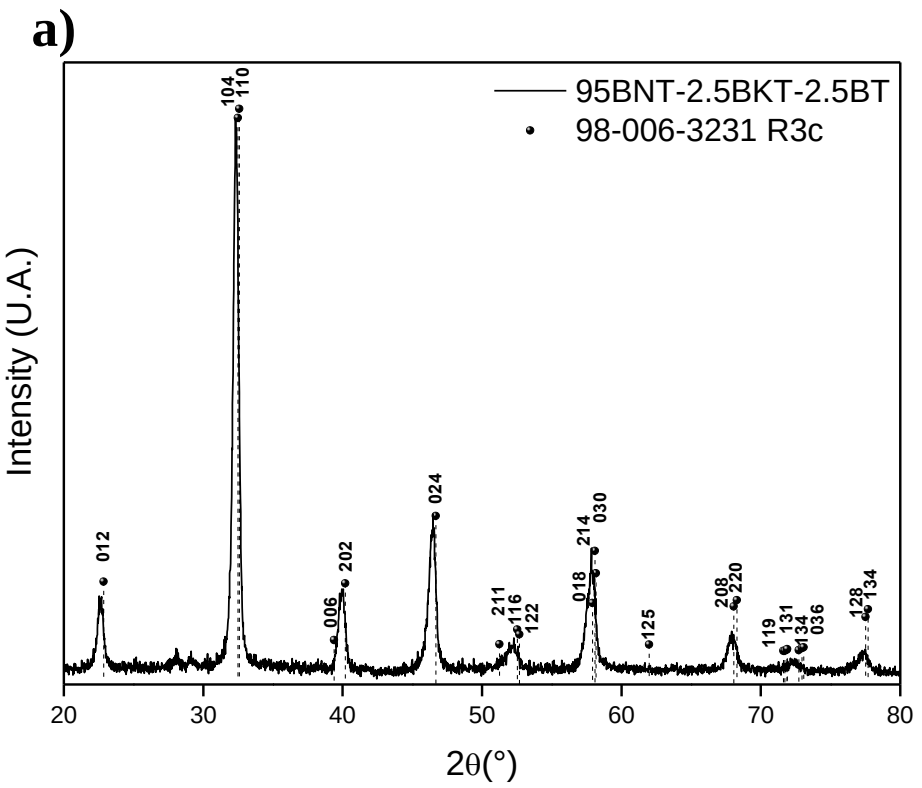

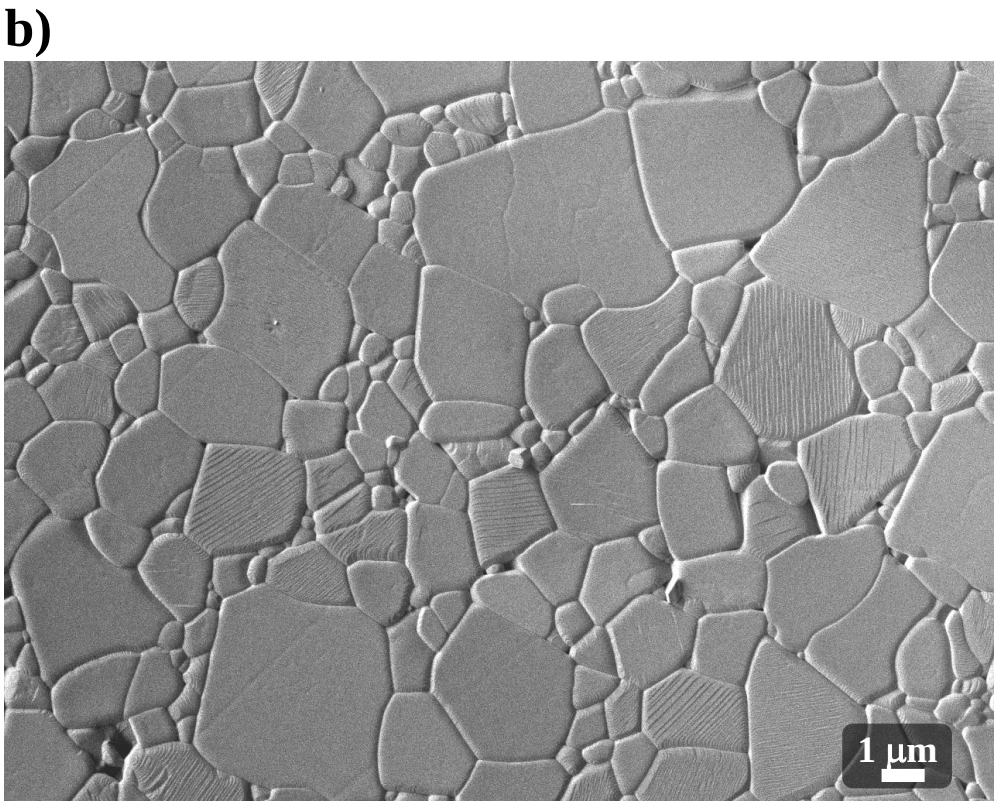

Fernández-Benavides et al., 2018

Figure 4.

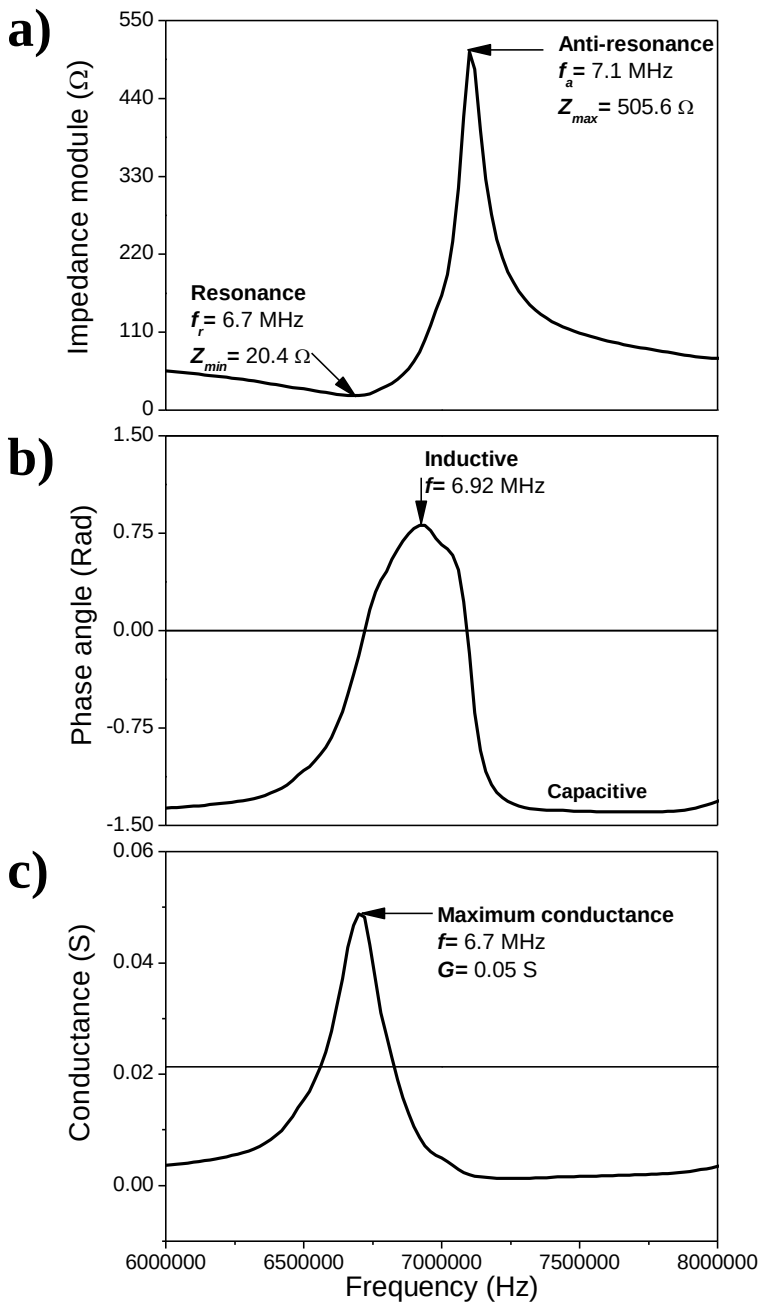

Fernández-Benavides et al., 2018

Figure 5.

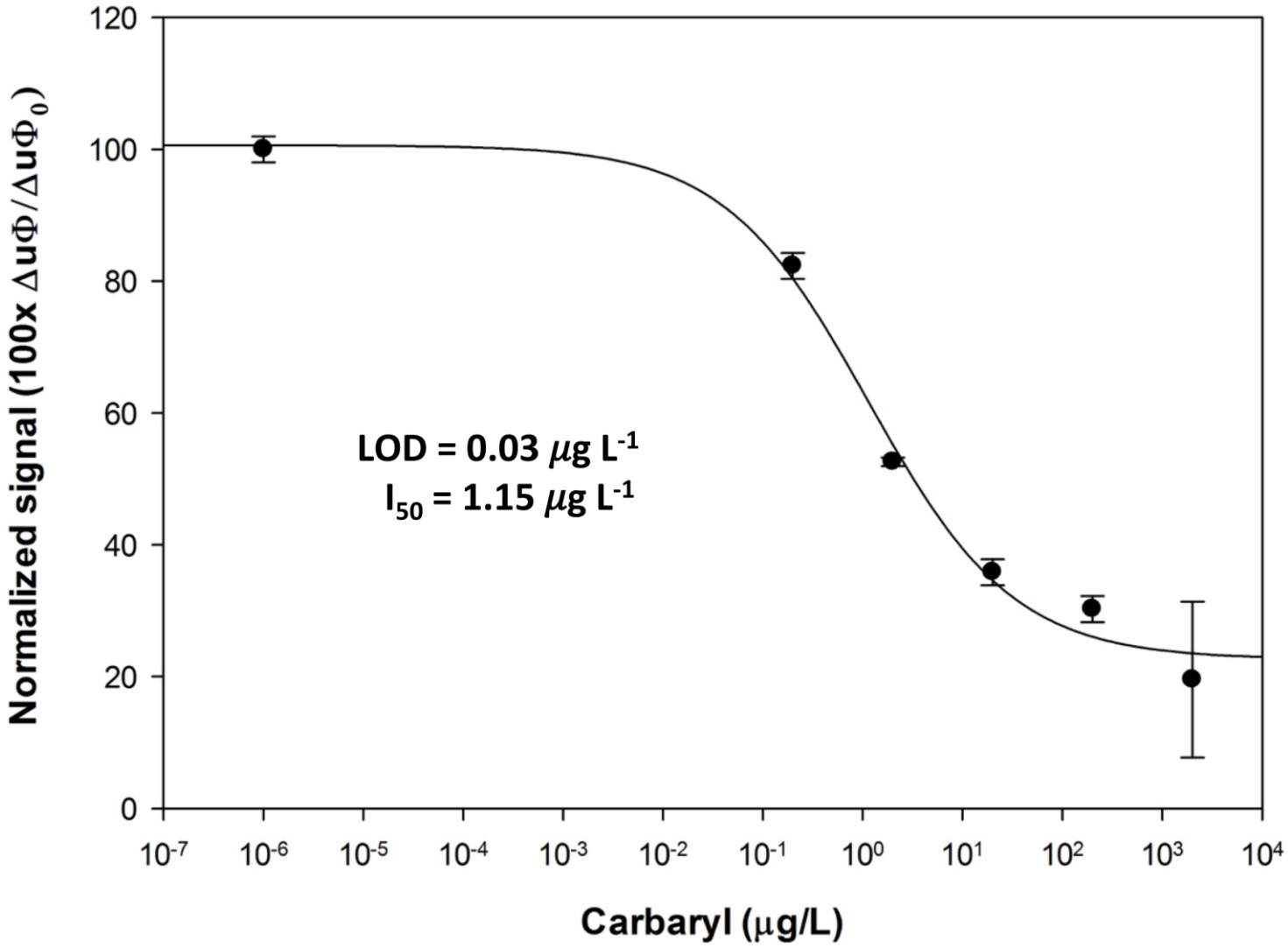

Fernández-Benavides et al., 2018